JOURNAL OF SOLID STATE CHEMISTRY 117, 136–144 (1995)

Compounds Based on the Vanadyl Formate Double Layer

Trevor R. Gilson

Department of Chemistry, University of Southampton, Southampton SO17 1BJ, United Kingdom

Received August 15, 1994; in revised form November 14, 1994; accepted November 21, 1994

New compounds, based on the interpenetrating double layers found in oxo-vanadium (IV) formate monohydrate, $VO(HCO_2)_2 \cdot H_2O$, have been synthesized. Ligand water is replaced by formic acid in $VO(HCO_2)_2 \cdot HCO_2H$, or by interlayer bridging fluoride with additional (NH_4 or K) cations in $[VO(HCO_2)_2]_2 \cdot NH_4F \cdot NH_4OH$, $[VO(HCO_2)_2]_2 \cdot KF \cdot NH_4OH$, and $[VO(HCO_2)_2]_2 \cdot KF \cdot \frac{1}{2}$ KOH. Indexed XRPD for the layer compounds and vibrational (IR and Raman) data including those for the related chain polymer $K_2VO(HCO_2)_2$ are given. Parallels are drawn with the lamellar phase vanadyl phosphates and arsenates. © 1995 Academic Press, Inc.

INTRODUCTION

Interest in intercalation hosts and other solid state materials formed by high oxidation-state transition elements (typically vanadium, molybdenum, or zirconium) and oxo-anions of (usually) second- or third-row main group elements, sometimes with additional cations, continues at a high level (1). It is instructive in this context to speculate on further generalizations of the structure type and to enquire whether carbon has any potential role as a "second element." While such materials are unlikely to have comparable temperature stability, great structural subtlety might be anticipated. Synthesis under acid conditions precludes carbonate or orthocarbonate anions, but carboxylates are more robust.

Most of the polymeric oxo-vanadium (IV) ("vanadyl") carboxylates have an unknown but apparently chain-based antiferromagnetic structure (2). By contrast the blue vanadyl formate $VO(HCO_2)_2 \cdot H_2O$ is magnetically normal and known (3) to have a pseudo-tetragonal sheet-based structure, in which a net of bridging formate groups links the equatorial position of linear $O{=}V{-}OH_2$ entities. It thus bears some resemblance to the α-phase (lamellar) vanadyl (IV or V) phosphates, arsenates, and sulfates, except that all the terminal oxygens lie on the same side of the sheet with dipole cancellation achieved by the formation of interpenetrating double layers. While direct intercalation has not been demonstrated, it is shown here that these double layers are capable of forming into a number of different solid state compounds with a close resemblance to an intercalation series.

The materials described in addition to the previously known monohydrate have all been characterized as single phases by X ray powder examination and are formulated as $VO(HCO_2)_2 \cdot HCO_2H$, $[VO(HCO_2)_2]_2 \cdot NH_4F \cdot NH_4OH$, $[VO(HCO_2)_2]_2 \cdot KF \cdot NH_4OH$, and $[VO(HCO_2)_2]_2 \cdot KF \cdot \frac{1}{2}$ KOH.

EXPERIMENTAL

While the production of good quality crystals of the monohydrate required hydrothermal conditions (3), a crude product was obtained by refluxing finely ground ammonium metavanadate in an excess of 75% formic acid for 24 hr with vigorous stirring. Regrinding may be necessary if "clumping" occurs. The polymeric nature of this material was evident in slow dissolution and reprecipitation, but it was purified by dissolving in boiling dilute (2 *M*) formic acid (ca. 20 g/liter) followed by slow evaporation of some 90% of the solvent. $VO(HCO_2)_2 \cdot H_2O$ found V, 28.9 (29.11), C, 13.9 (13.73), H, 2.2 (2.30).

$VO(HCO_2)_2 \cdot HCO_2H$ and the ammonium and mixed ammonium/potassium fluoride adducts were prepared initially by a melt method. Ammonium formate was fluxed with a small (1–5%) proportion of formic acid and held at 150–160°C. Vanadyl formate hydrate dissolved easily in this melt, working at a convenient dilution of ca. 1 in 10 g, or alternatively ammonium metavanadate was reduced to an identical V(IV) composition in about an hour; ideally the experimental arrangements retained the slightly volatile ammonium formate, but water was allowed to escape. Additional formic acid was dripped in as the melt became too viscous to stir at this temperature (it may reversibly darken if this addition is inadequate, but the b.p. should not drop below 150°). Heating and stirring were continued until slightly past the pure blue V(IV) stage, with a degree of green coloration signaling complete dehydration and the onset of reduction to V(III).

The formic acid adduct was prepared from the hot melt by dripping in anhydrous formic acid at a faster rate while

0022-4596/95 $6.00

continuing to stir; precipitation was complete when the boiling point had dropped to ca. 105°. $VO(HCO_2)_2 \cdot HCO_2H$ found V 24.4 (25.09), C 17.65 (17.75), H 1.8 (1.99).

The diammonium form of the fluoride was prepared by adding ammonium fluoride (1:1 mole ratio with V) to the melt before the addition of formic acid, and the mixed ammonium/potassium material likewise by adding potassium fluoride. In the case of the fluorides, it was not necessary for the diluent formic acid to be rigorously anhydrous and reagent grade 98–100% sufficed. The hydrate also was obtainable from the initial melt by addition of 2 M formic acid.

The melt-prepared fluorides generally showed high carbon content and were thought to contain occluded formic acid. X ray and IR examination showed conclusively that the products were identical to those below.

Purer forms of the first two fluorides and the per-potassium compound were prepared in finely divided form from the formic acid adduct by warming the finely ground material in 5–10 volumes of anhydrous formic acid with appropriate fluorides, to a total mole ratio of ca. 4 with vanadium. The mixed potassium ammonium compound formed preferentially both in formic acid and in the melt, until such time as one cation or the other was used up.

In all cases the solid products were filtered at the pump and washed with formic acid. Long term storage was enhanced by the presence of acid residues. $[VO(HCO_2)_2]_2 \cdot NH_4F \cdot NH_4OH$ found V 26.4 (26.39), C 12.5 (12.45), H 3.3 (3.39), N 7.4 (7.26), F 4.2 (4.24). $[VO(HCO_2)_2]_2 \cdot KF \cdot NH_4OH$ found V 24.0 (25.6), C 13.1 (12.07), H 2.0 (2.28), N 3.3 (3.52), K 9.6 (9.82), F 5.3 (4.77). $[VO(HCO_2)_2]_2 \cdot KF \cdot \frac{1}{2} KOH$ found V 25.1 (25.46), C 11.0 (12.01), H 0.9 (1.13), K 14.5 (14.66), F 4.3 (4.75).

INSTRUMENTATION

X ray powder diffraction (XRPD) patterns were obtained on a Phillips PW 1730/10 ($VO(HCO_2)_2 \cdot H_2O$, $VO(HCO_2)_2 \cdot HCO_2H$, and $[VO(HCO_2)_2]_2 \cdot KF \cdot NH_4OH$), a Siemens Diffrac 500 diffractometer ($[VO(HCO_2)_2]_2 \cdot NH_4F \cdot NH_4OH$), or on an Inel Diffractinel area detector instrument ($[VO(HCO_2)_2]_2 \cdot KF \cdot \frac{1}{2} KOH$), all using Cu$K\alpha$ radiation and calibrated with Si. Precision of the observed *d*-spacings may be judged from consistency with the calculated values for nonoverlapping reflections. Accuracy is believed to exceed the quoted precision of 0.001 Å for later values and in the case of the first two instruments, giving cell dimensions accurate to ± 0.003 Å (0.01 Å in the case of the Diffractinel). Infrared spectra were obtained on a variety of standard Perkin–Elmer instruments, using Nujol or perfluorokerosene mulls. Raman spectra were obtained using a Coderg T800 triple monochromator with Ar^+ laser excitation, most usefully at 457.9 nm.

CHARACTERIZATION

The identity of the monohydrate prepared above, with the hydrothermal material was established by XRPD and simulation using the published (3) structure. Routine characterization and refinement of the preparative procedures were conveniently carried out by examination of the IR spectrum, particularly the OH/NH stretching region above 3000 cm^{-1}, as well as by XRPD. Coordinated water and formic acid and the ammonium cation all fall in the "medium" hydrogen bonding régime in which the corresponding hydrogenic vibrations are narrowed, so that all show a characteristic and easily recognized signature in this region (Fig. 1, Table 1). The monohydrate is a thermodynamic sink in this system (although less so in the presence of ammonium fluoride) and is the common impurity detected easily by both XRPD and IR. There is no evidence for phases intermediate between those listed. A sample XRPD pattern is shown for the compound $[VO(HCO_2)_2]_2 \cdot NH_4F \cdot NH_4OH$ (Fig. 2).

Analysis for fluoride was both by colorimetric methods (with preextraction of the vanadium into oxine reagent) (4) and by ion-selective electrode. Potassium was determined by flame photometry. Vanadium was determined by ignition of V(V) in air, using in the case of fluoride-containing materials preadmixture with a weighed excess of dried (160°C) potassium carbonate and a platinum crucible. Separate experiments established that carbon dioxide

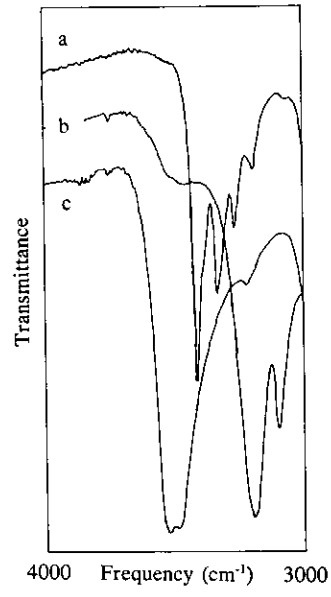

FIG. 1. The infrared spectra of (a) $VO(HCO_2)_2 \cdot HCO_2H$, (b) $[VO(HCO_2)_2]_2 \cdot NH_4F \cdot NH_4OH$, and (c) $VO(HCO_2)_2 \cdot H_2O$ in the region 3000–4000 cm^{-1}. The two potassium-substituted fluorides show respectively decreased ($K \cdot NH_4$) or absent ($K_{1.5}$) NH stretching bands at 3190 and 3092 cm^{-1} (Table 1).

TABLE 1
Infrared and Raman Spectra (Solids) 350–4000 cm^{-1} (±2 cm^{-1})

$VO(HCO_2)_2 \cdot H_2O$		$VO(HCO_2)_2 \cdot HCO_2H$		$[VO(HCO_2)_2]_2 \cdot NH_4F \cdot NH_4OH$		$[VO(HCO_2)_2]_2 \cdot KF \cdot NH_4OH$		$[VO(HCO_2)_2]_2 \cdot KF \cdot \frac{1}{2}KOH$		$K_2VO(HCO_2)_4$		$HVO(HCO_2)_3$, $0.33KH(HCO_2)_2$	
IR	Raman	IR	Raman	IR	Raman	IR	Raman	IR	Raman	IR	Raman	IR	
380sh	361w	370sh	363w	361mw	368m	365mw	368m	367mw					V-bridging formate
440s,br	393sh	380w	384vw	371mw		375mw		375mw		388s	380w	390sh	stretches
	430mw	436s	425mw	423s	410mw	422s	406m	424s		425sh	400sh	450s	
				483m		487m		485m					ν VF
640m,br		635m	630w	540wsh		540wsh		540wsh					OH_2 torsion/3op OH
										798m			
845m	844w	842m	840w	843m	846w	843m	845w	842m	845w	807m	805w	812m	δCO_2
						920vw	920w	920vw	920w				
992s	983vs	987s	980vs	973s	977s	976s	978s	976s	976s	961s	961vs	990s	ν v = 0
1077vw	1080vw	1050w	1077vw	1020vw		1020vw	1080w	1020vw			1057w		δ CH op
		1078vw		1080vw	1078w			1075vw					
		1100w	1100w										
										1289ms		1245vw,br	
										1299ms	1295m		Monodentate formate (see text)
										1318s	1325w		
1361s	1358w	1360s	1329w	1362s	1358wsh	1370s	1346w	1372s		1344m	1343m	1370s	$\nu_s CO_2$ + δ CH ip
							1362wsh			1370wbr	1359m		
1382ms	1371w	1382ms	1386s	1383sh	1385s	1385sh	1384vs	1385sh	1382vs		1379m		
	1386s									1397w	1396ms		
				1441mw	1437wsh	1441w							δNH_4^+
1570vs,br	1569w	1575vs	1567w	1585vs	1570mw	1585vs	1571mw	1585vs	1567w	1587sh	1585w	1670vs	$\nu_{as} CO_2$
										1608sh	1596vvw	1605sh	
										1620vs	1623w	1665sh	
										1641sh	1651m		
											1666vw		
1625sh	1624vw		1605vw										δOH_2
		1715s	1676w		1695vwbr		1692vwbr					1720m	ν C-O formic acid
					2150vw								?
2880w	2882m		2879m		2878m		2882m		2881m	2880w	2854m		ν OH bridging formate or
											2873m		
2940mw	2949wbr		2924m[a]		2948w		2955w		2955w	2933m,br	2896sh		(a) formic acid
			2950wbr										
3200sh		3195w		3092w	3114w	3093w							
		3266mw	3266w										ν OH or νNH_4^+
3460mssh	3449w	3310sh	3303w	3190m	3196w	3193mw							
		3330m	3330w										
3515ms	3519vw	3380sh		3460w?		3460w?		3460w?					
		3414s	3414mw										

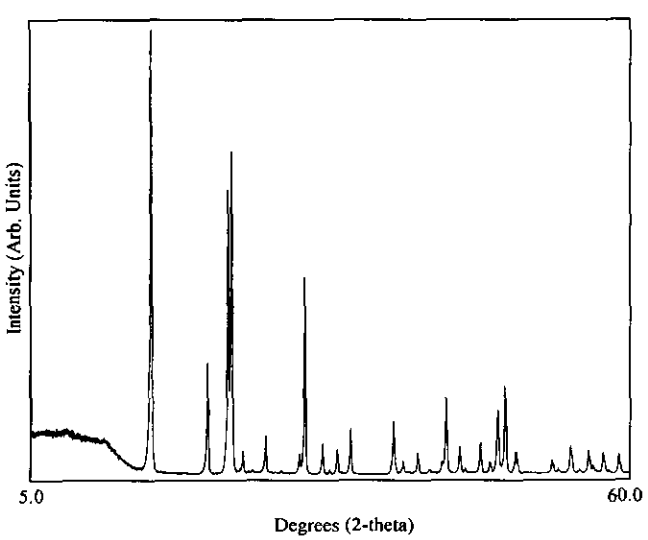

FIG. 2. The XRPD pattern for $[VO(HCO_2)_2]_2 \cdot NH_4F \cdot NH_4OH$ (Cu$K\alpha$1 + $K\alpha$2). Monochromated-radiation scans of selected areas failed to show any splitting of the pseudo-tetragonal a dimension.

was released in 1:1 mole ratio F:CO_2 by fluoride, and in 1:1.25 ratio V:CO_2 by vanadium under these conditions. Some confirmatory volumetric determinations were also carried out.

PROPERTIES

Vibrational spectra are listed in Table 1, together with data for the related double-salt $K_2VO(HCO_2)_4$ (5) and its amorphous formic acid reaction product $HVO(HCO_2)_3$,$0.33KH(HCO_2)_2$, for comparison. XRPD data are listed in Tables 2–5.

These materials are all indefinitely stable in the presence of formic acid residues, but may undergo slow, initially superficial air oxidation otherwise. All darken at 2–300°C before melting, and IR spectroscopy in the OH stretching region shows that initial darkening of the monohydrate is due to disproportionation to the formic acid adduct and, presumably, VO_2 accompanying dehy-

TABLE 2
Observed and Calculated XRPD for $VO(HCO_2)_2 \cdot HCO_2H$

h	k	l	d(obs) Å	d(calc) Å	I(obs)[a]	I(calc)[b]
0	0	2	9.891	9.887	35.5	38.2
1	1	2	5.105	5.104	100.0	100.0
0	0	4	4.944	4.944	26.8	21.6
2	0	0	4.226	4.225	27.4	18.2
0	2	0	4.203	4.204		18.2
2	0	1	4.131	4.131	1.6	1.3
2	0	2	3.890	3.885	4.2	0.1
0	2	2	3.870	3.868		0.1
1	1	4	3.803	3.805	29.9	34.9
1	2	0	3.760	3.764	3.3	1.7
1	2	1	3.697	3.697	1.7	1.7
2	0	3	3.556	3.557	4.3	0.5
2	1	2	3.527	3.527		1.7
0	0	6	3.295	3.296	20.5	18.9
2	0	4	3.208	3.212	8.5	4.8
0	2	4		3.202		4.6
2	2	0	2.980	2.980	40.4	42.8
2	2	1	2.949	2.947	1.5	0.6
2	0	5	2.885	2.887	0.7	0.1
2	2	2	2.852	2.853	2.2	2.6
3	1	0	2.676	2.670	3.0	0.1
3	1	2	2.576	2.578	7.3	4.3
1	3	2		2.569		4.3
1	2	6	2.479	2.479	3.3	0.3
3	1	4	2.351	2.350	8.7	3.2
1	3	4	2.341	2.342		3.2
1	1	8	2.281	2.283	15.7	9.0
2	2	6	2.208	2.210	5.7	3.8
4	0	0	2.114	2.112	12.1	4.2
0	4	0	2.103	2.102		4.1
3	1	6	2.068	2.075	1.0	0.5
1	3	6		2.070		0.5
2	1	8		2.068		0.1
4	0	2		2.066		0.6
1	4	0	2.038	2.040	0.8	0.3
4	0	3	2.010	2.012	1.0	0.1
2	3	5		2.011		0.1
4	1	2		2.006		0.5
0	0	10	1.977	1.977	4.6	4.0
3	3	2	1.947	1.948	6.4	7.1
4	2	0	1.886	1.887	15.5	5.6
2	4	0		1.882		5.5
3	3	4	1.843	1.843	2.4	3.3
3	1	8	1.813	1.814	2.8	1.8
1	3	8		1.811		1.7
2	0	10	1.786	1.791	1.6	0.7
0	2	10		1.789		0.8
4	0	6		1.778		0.6
0	4	6	1.767	1.772	2.5	0.6
4	2	4		1.763		0.2
2	4	4		1.759		0.2
2	3	8	1.698	1.697	1.2	0.1
0	0	12	1.646	1.648	11.6	1.1
2	2	10		1.648		2.8
4	2	6	1.635	1.638		1.2
2	4	6		1.634		1.1
5	1	2		1.634		2.6
1	5	2	1.624	1.627		2.6
3	1	10	1.587	1.589	0.7	1.5
1	3	10		1.587		1.5
5	1	4	1.568	1.571	2.3	1.4
1	5	4		1.564		1.3
3	3	8	1.547	1.548	1.5	2.2
4	4	0	1.490	1.490	1.3	1.7
2	2	12	1.442	1.442	8.0	1.7
5	3	2	1.430	1.432		1.3
3	5	2		1.429		1.3
5	1	8	1.374	1.376	7.1	1.1
1	1	14		1.374		0.9
1	5	8		1.372		1.1
4	2	10	1.364	1.365		0.9
2	4	10		1.363		0.9
4	4	6		1.358		0.6
6	2	0	1.336	1.335	3.9	1.1
2	6	0	1.329	1.330		1.0
5	3	8	1.247	1.249	4.3	0.6
3	1	14		1.249		0.5
1	3	14		1.247		0.5
3	5	8		1.247		0.6
4	2	12	1.234	1.241		0.9
2	4	12		1.240		0.9
6	2	6		1.238		0.5
2	6	6		1.233		0.5

[a] Integrated intensities scaled to (112) = 100.0

[b] Calculated intensities refer to an unrefined model in which monohydrate-like double layers were accommodated to the opposite orthorhombic cell distortion observed in this case and placed in translational register. Ligand formic acid was placed in plausible but unconfirmed positions in the interlayers, in such a way as to double the vertical cell dimension under space group $P2_122_1$.

dration:

$$3\ VO(HCO_2)_2 \cdot H_2O = 2\ VO(HCO_2)_2 \cdot HCO_2H + VO_2 + 2\ H_2O. \quad [1]$$

Remarkably, the fluoride materials are stable to well over 200°C *in vacuo*.

Boiling in excess water results in partial or complete decomposition to the monohydrate. No reaction is observed with monoalcohols, but both the hydrate and (better) the formic acid adduct form complex solid state condensation products on heating with anhydrous 1:2 and 1:3 diols. These materials have well-characterized IR spectra, but are only partially crystalline and hydrolyze cleanly to V(IV) in aqueous mineral acid. They are the subject of further investigation.

X RAY STUDIES AND STRUCTURAL INFERENCES

Of the new materials described here, only the formic acid adduct, $VO(HCO_2)_2 \cdot HCO_2H$, has been grown in crystals large enough for conventional X ray examination and such crystals all appeared to be microdomain twinned

TABLE 3
Observed and Calculated XRPD for
$[VO(HCO_2)_2]_2 \cdot NH_4F \cdot NH_4OH$

h	*k*	*l*	*d*(obs) Å	*d*(calc) Å	*I*(obs)[a]	*I*(calc)[b]
0	0	2	7.592	7.617	1.5	2.2
1	1	1	5.551	5.536	100.0	100.0
2	0	0	4.210	4.202	25.1	9.9 + 11.7
1	1	3	3.866	3.860	64.2	55.5
0	0	4	3.814	3.809	72.8	78.7
1	2	1	3.654	3.649	5.2	1.5
2	1	2	3.372	3.370	8.4	4.2
1	2	3	3.024	3.021	3.3	2.5
2	2	0	2.973	2.971	43.8	50.2
2	0	4	2.823	2.822	7.2	4.9 + 5.4
2	2	2	2.770	2.768	1.2	1.3
1	1	5	2.713	2.711	5.8	3.8
3	1	1	2.619	2.618	10.4	4.7 + 4.6
3	1	3	2.355	2.355	12.0	8.2 + 7.7
3	2	1	2.304	2.304	2.9	4.7
2	3	2	2.230	2.229	7.3	8.4
2	0	6	2.174	2.173	1.2	1.0 + 1.3
3	2	3	2.117	2.118	2.3	3.8
4	0	0	2.101	2.101	15.9	5.8 + 5.6
1	1	7	2.043	2.044	6.1	8.1
1	4	1	2.022	2.020	1.2	1.3
3	3	1	1.964	1.964	7.0	5.2
2	2	6	1.930	1.930	2.5	3.8
0	0	8	1.904	1.904	13.5	13.4
4	2	0	1.879	1.879	19.0	9.7 + 9.8
3	3	3	1.845	1.845	5.0	5.2
4	0	4	1.841	1.840	5.0	0.4 + 0.4
2	0	8	1.734	1.734	3.1	0.9 + 0.9
2	3	6	1.716	1.717	1.3	2.2
4	2	4	1.684	1.685	6.1	1.7 + 1.6
3	1	7		1.684		3.1 + 3.4
3	3	5	1.660	1.661	1.1	0.8
5	1	1	1.638	1.639	4.8	3.0 + 2.9
1	1	9	1.628	1.628	2.2	0.3
2	2	8	1.603	1.603	4.6	5.9
3	2	7	1.589	1.591	1.1	1.0
4	1	6		1.589		0.7
5	1	3	1.567	1.568	4.4	3.3 + 3.4

[a] Scaled peak heights.

[b] Calculated intensities refer to an unrefined model in which monohydrate-like double layers were accommodated to the undistorted cell observed in this case and placed in appropriate register for space group *Ccca* (see text), with symmetrical linear fluorine bridges. Cations and the hydroxide ion were placed in appropriate but unconfirmed general and special positions respectively of the subgroup *Ccc*2 (identical cell), here reset to *Bb2b* to emphasise the relationship to tetragonal indexing. Where two calculated intensities are shown, the second refers to the allowed overlapping (*khl*) reflection.

(as with the hydrate when grown under nonhydrothermal conditions). A reason for this phenomenon is suggested below, but it was possible to validate the cell dimensions and other inferences obtained from the powder pattern using imperfect single crystal data. These structures present a number of difficulties in the way of complete elucidation by XRPD, but the overall arrangement is quite clear. Apart from the usual accidental overlap problems, the partial or complete merging of (*hkl*) with (*khl*) reflections and the strong pseudo-symmetry of the structural skeleton make determination of the true space group almost impossible. It is not even certain that the space group assigned (3) to the hydrate is conformed to by the water protons.

Rietveld refinement could have been performed using the most probable space groups, but it is likely that the differences in residuals between alternative space groups would have been insufficient to allow a definite decision. In the case of the formic acid adduct, there are simply too many parameters to refine using X ray powder data alone, but it is worth noting that the structure of the marginally simpler hydrate was determined from powder data in this laboratory before the single-crystal determination (3) became available. This was done using a variant (6) of the Rietveld method in which overlapped reflections are recursively reallocated from the current model, thus avoiding the problem of zone-dependent peak shape, although the radius of applicability is smaller. Probably the elegant new methods (7) in which X ray and neutron data are refined simultaneously would be required to solve these structures completely.

In the absence of neutron data, the approach adopted was to simulate the X ray pattern using "double-layer" parameters derived from the hydrate, allowing only for the differing twist angle determined from the pseudo-tetragonal *a* dimension. It will be seen (Tables 2–5) that remarkably good fits were obtained, leaving little doubt that the models used were qualitatively correct.

An idealized isolated tetragonal sheet from the monohydrate (3) is shown in Fig. 3, together with the hydrogen-bonded water ligands from the layer above. A favorable value for the VOC angle is obtained by means of an alternating twist of the VO_4 centers about a vertical axis. These sheets back up to one another in staggered fashion, such that the two layers of oxo-oxygens interpenetrate to the extent of a nearly equal *z* coordinate. This results in an orthorhombic double layer (Space group *Pcca*) but with little impetus to differentiate the tetragonal cell dimension of ca. 8.4 Å. The translational relationship of the two sheets vis-a-vis the twist sequence decides the resultant orthorhombic symmetry axis directions, and any irregularity of twist sequence within a single sheet would result in apparent twinning of the double layer. In the hydrate or aquoadduct, a simple translational succession of double layers builds up, with the result that vanadium atoms in the contiguous single sheets are also staggered across the ligand–ligand interface and the water ligands hydrogen bond to the formate of that contiguous layer as shown. A stereoscopic view of this structure is shown in (3). Given the observed differentiation of ca. 0.1 Å in the cell dimension, it is possible that the water protons conform

TABLE 4
Observed XRPD for $[VO(HCO_2)_2]_2 \cdot NH_4F \cdot KOH$

h	*k*	*l*[a]	*d*(obs) Å	*d*(calc) Å	*I*(obs)[b]
0	0	2	7.844	7.782	4.7
1	1	1	5.529	5.498	53.5
#2	0	0	4.171	4.156	32.9
0	0	4	3.888	3.891	100.0
1	1	3		3.890	
#2	0	2	3.669	3.666	2.2
1	2	1	3.623	3.616	3.8
2	1	2	3.361	3.354	5.1
1	2	3	3.025	3.022	2.5
2	2	0	2.941	2.939	30.1
#2	0	4	2.837	2.840	6.3
1	1	5		2.751	7.0
2	2	2		2.749	
0	0	6	2.593	2.594	3.5
#3	1	1		2.592	
2	2	4	2.345	2.345	14.2
#3	1	3		2.345	
3	2	1	2.279	2.280	1.9
2	3	2	2.204	2.210	2.2
#2	0	6		2.201	
3	2	3	2.107	2.107	2.2
1	1	7	2.078	2.080	14.9
#4	0	0		2.078	
#1	3	5	2.006	2.008	1.9
#4	0	2		2.008	
1	4	1		1.999	
4	1	2	1.943	1.952	10.8
0	0	8		1.945	
2	2	6		1.945	
3	3	1		1.944	
#2	4	0	1.859	1.859	14.2
#4	0	4	1.833	1.833	4.4
3	3	3		1.833	
#2	0	8	1.759	1.762	2.5
#3	1	7	1.695	1.698	1.3
1	4	5		1.692	
#4	2	4	1.676	1.677	0.9
3	3	5	1.656	1.658	0.9
3	4	1		1.653	
4	3	2	1.628	1.626	4.7
2	2	8		1.622	
#4	0	6		1.622	
#5	1	1		1.621	
0	0	10	1.554	1.556	3.2
#5	1	3		1.555	
3	3	7	1.467	1.470	1.3
4	4	0		1.469	
3	4	5		1.466	
#5	1	5	1.441	1.444	0.9
2	1	10		1.436	
#4	0	8	1.418	1.420	3.8
#5	3	1		1.420	
#6	0	0	1.385	1.385	2.5
3	2	9		1.383	
5	2	5		1.383	
#4	2	8	1.341	1.344	3.8
#5	1	7	1.312	1.315	2.8
#6	2	0		1.314	
1	4	9		1.313	

TABLE 4—*Continued*

[a] Indexing relates to *Bbab* setting of possible space group *Ccca*. Indexes preceeded by hash (#) are overlapped by the *Bbab* allowed (*khl*).
[b] Scaled peak heights.

only to a lower space group (e.g., $P222_1$) with a less symmetrically bifurcated hydrogen bond.

It is not unexpected that a series of comparable compounds should result from the substitution of the relatively lightly coordinated ligand to vanadium trans to the oxo-oxygen and it is certain that the compounds described here constitute such a series. The identifying feature for the pseudo-tetragonal double-layer structural unit is taken to be the characteristic series of medium intensity (*hk*0) reflections ($h = 2n$, $k = 2n$) in the XRPD pattern (Table 6), with a corresponding cell dimension of 8.3–8.5 Å, which may be close doublets ($h \neq k$ only) where external influences cause the cell dimensions to differentiate. The smaller cells (Table 7) must correspond to an increase in the twist angle. The characteristic intensity sequence for the (*hk*0) reflections of the lighter compounds (Table 6) is somewhat overlaid in those which contain potassium, in line with trial simulations (8), but the overall pattern leaves little doubt but that the latter are isostructural with $[VO(HCO_2)_2]_2 \cdot NH_4F \cdot NH_4OH$. In practice a new candidate compound may rapidly be screened by examination of the IR, where a very simple spectrum is expected with certain pointers (V=O stretch > 970 cm^{-1}, an intense formate band at 1360–1370 cm^{-1}, and the OCO deformation > 840 cm^{-1}). These values may be compared with the rather different ones found for the related chain-polymer $K_2VO(HCO_2)_4$ (5) (Table 1). It is found also that monodentate formate has a strong band at 1250–1300 cm^{-1} in all cases examined, and this difference is proposed as diagnostic.

It has been assumed that the thickness of a double layer remains constant to a first approximation in interpreting the observed pseudo-tetragonal *c* dimensions.

It is at once clear that the formic acid adduct conforms to this general pattern, with a reasonable increase of 2.5 Å in (double-layer to double-layer) spacing over the aquo compound and a poorly marked repeat of two double layers rather than one. Trial simulations (8) (Table 2) confirm the resulting overall intensity pattern, without being able to refine the skeleton or to pinpoint the exact ligand geometry. This structure is thus qualitatively identical to the hydrate (Fig. 3 and Ref. 3), but with the formic acid ligand replacing water. No doubt a stabilizing hydrogen bonding pattern also establishes itself here.

TABLE 5
Observed XRPD for $[VO(HCO_2)_2]_2 \cdot KF \cdot \frac{1}{2}KOH$

h	k	l^a	d(obs) Å	d(calc) Å	I(obs)^b
0	0	2	7.73	7.76	3.2
1	1	1	5.449	5.470	14.6
#2	0	0	4.116	4.133	14.0
0	0	4	3.870	3.878	100.0
1	1	3		3.873	
#2	0	2	3.641	3.647	1.1
1	2	1	3.588	3.596	1.9
2	1	2	3.338	3.337	4.1
1	2	3	3.009	3.007	1.2
2	2	0	2.923	2.922	13.5
#2	0	4	2.827	2.828	4.4
1	1	5	2.741	2.740	6.7
2	2	2		2.735	
#3	1	1	2.575	2.578	2.2
2	2	4	2.330	2.334	9.2
#3	1	3		2.333	
3	2	1	2.263	2.268	0.6
#2	0	6	2.194	2.192	4.1
1	1	7	2.066	2.072	12.0
#4	0	0		2.066	
#1	3	5	1.999	1.999	1.8
#4	0	2		1.997	
4	1	2	1.939	1.941	16.3
0	0	8		1.939	
#4	2	0	1.848	1.848	9.9
#4	0	4	1.823	1.824	4.3
3	3	3		1.823	
#2	0	8	1.757	1.755	5.8
1	1	9	1.654	1.653	0.9
4	3	2	1.614	1.617	1.7
2	2	8		1.616	
#4	0	6		1.614	
#5	1	3	1.547	1.547	2.5
0	0	10		1.551	
#5	3	1	1.413	1.412	2.4
#4	2	8	1.337	1.338	2.4
#5	1	7	1.306	1.308	1.9
#6	2	0		1.307	
1	4	9		1.307	

[a] Indexing relates to *Bbab* setting of possible space group *Ccca*. Indexes preceeded by hash (#) are overlapped by the *Bbab* allowed (*khl*).
[b] Scaled peak heights.

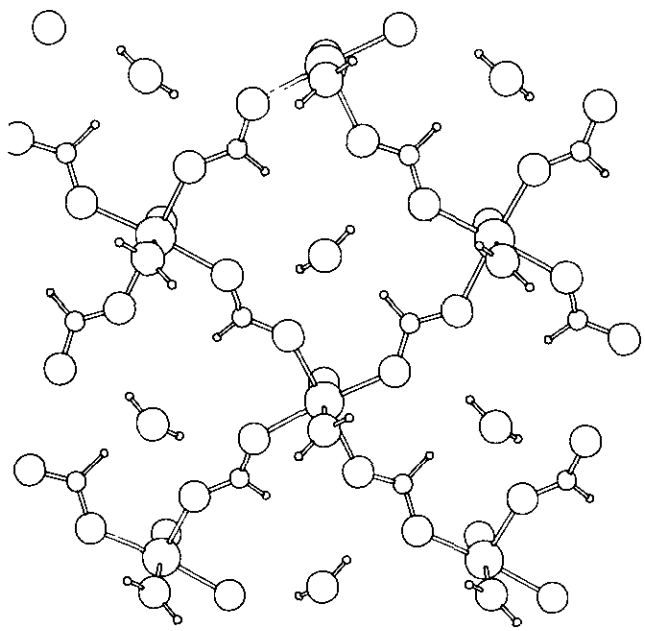

FIG. 3. An isolated idealized tetragonal sheet from the structure of $VO(HCO_2)_2 \cdot H_2O$ (3). Hydrogen-bonded water ligands from the contiguous sheet are also shown. Atoms are coded in conventional (atomic no.) size order H < C < O < V.

By contrast the fluorides show a dominant repeat of two double layers and a much-changed centered-lattice intensity pattern in the non-(*hk*0) reflections, which must result from an eclipsed positioning of the vanadium atoms in contiguous single sheets across the "ligand gap." Chemical principles and an inspection of the formulas suggest a linear V–F–V bridge between the layers (Fig. 4), which is supported by a V–V distance of ca. 4.2 Å (again making the assumption that the double-layer thickness is approximately constant), and a new infrared frequency of 485 cm^{-1} not present in the first two compounds. There is no apparent doubling of the ($h \neq k$) reflections in this case, strengthening the supposition that ligand side asymmetries cause the cell perturbation in the nonfluoride compounds.

It may be noted that interlayer voids form between the fluorine atoms in this skeleton and that, depending on the

TABLE 6
Relative Intensities for the (*hk*0) ($h = 2n$, $k = 2n$) Characteristic Series of XRPD Reflections

(200)	(220)	(400)	(420)	(440)	(600)	(620)	(640)	Relative to[a]
16	38	11	14	1	0	7	8	(111) = 100 $VO(HCO_2)_2 \cdot H_2O$
27	40	12	16	1	0	4	—	(112) = 100 $VO(HCO_2)_2 \cdot HCO_2H$
25	44	16	19	—	0	4	—	(111) = 100 $[VO(HCO_2)_2]_2 \cdot NH_4F \cdot NH_4OH$
33	30	15	14	1	—	3	—	(004) = 100 $[VO(HCO_2)_2]_2 \cdot KF \cdot NH_4OH$
14	14	12	10	2	—	—	—	(004) = 100 $[VO(HCO_2)_2]_2 \cdot KF \cdot \frac{1}{2}KOH$

[a] Note that (111) and (112) are structurally comparable reflections for the first two compounds, whereas the prominence of (111) in the fluorides, also with a doubled interlayer repeat, reflects the changed layering pattern. No attempt has been made to apportion overlapping reflections.

TABLE 7
Cell Dimensions (Å), Densities (ρ, kg · dl^{-3}), and Formula Weight (MW, amu)

	a *Pbab*[a]	*b* *Pbab*[a]	(*a* + *b*)/2	*c*	*c'*[b]	ρ[c]	MW obs	MW calc
$VO(HCO_2)_2 \cdot H_2O$[d]	8.395(2)	8.510(1)	8.453	7.433(1)	7.433	2.20	176 ($Z = 4$)	174.99
$VO(HCO_2)_2 \cdot HCO_2H$	8.449(3)	8.407(3)	8.428	19.774(6)	9.887	1.90	201 ($Z = 8$)	203.00
$[VO(HCO_2)_2]_2 \cdot NH_4F \cdot NH_4OH$			8.404(3)	15.234(5)	7.62	>2.1	>340 ($Z = 4$)	386.03
$[VO(HCO_2)_2]_2 \cdot KF \cdot NH_4OH$			8.312(3)	15.564(5)	7.78	>2.2	>356 ($Z = 4$)	398.02
$[VO(HCO_2)_2]_2 \cdot KF \cdot \frac{1}{2}KOH$			8.266(10)	15.514(15)	7.76	>2.3	>367 ($Z = 4$)	400.10

[a] *Pbab* is an unconventional setting of *Pcca*, chosen to emphasize the relationship to tetragonal pseudo-symmetry. It is not implied that the formic acid adduct is of full *Pcca* symmetry, but the distortion from equal *a* and *b* is in the opposite direction as shown.

[b] *c'* is the vertical distance from one double layer to another, irrespective of translation in the plane and minor changes in ligand geometry.

[c] Densities were determined by flotation and are included to show the origin of the assigned values for *z*. Uncertainties are greater (but hard to quantify) in the case of the microcrystalline fluorides.

[d] Ref. (3).

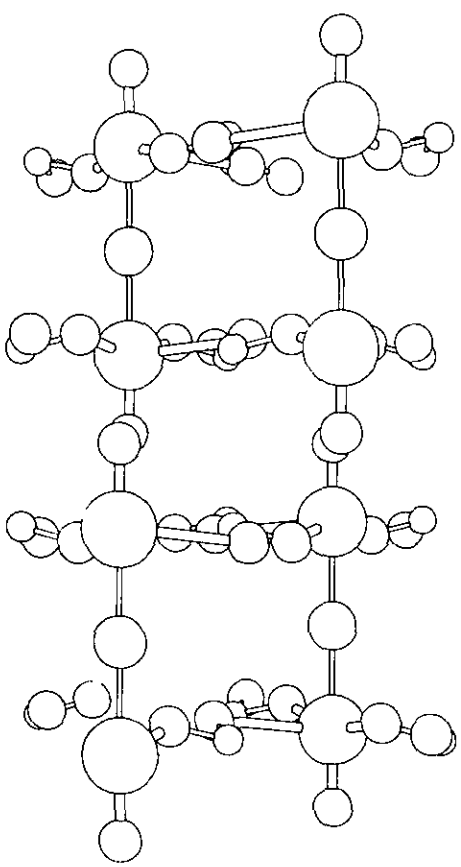

FIG. 4. Layer sequence for the $[VO(HCO_2)_2]_2F^-$ skeleton of the isomorphous $[VO(HCO_2)_2]_2 \cdot MF \cdot M'OH$ series of compounds. Alternate interlayers show (i) bridging fluorine, and (ii) the interpenetrating terminal oxygens from above and below. Fluorine atoms are conventionally size-coded between oxygen and vanadium.

relationships of the fluorine-bridged vanadium centers, these are of approximately *D2d* (staggered twists) or *D2h* (eclipsed twist) symmetry with idealized skeletal space group *Ccca* or *Cmca* respectively. Although the *Ccca* (staggered twists) option is preferred, both from trial simulation results and from the lack of cell distortion, it has been possible neither to decide definitely between these possibilities nor to locate unambiguously the ammonium or potassium cations (up to two per void) and the additional anion which they must accommodate. The staggered form of the void is shown in Fig. 5. It is noted that the experimentally observed stoichiometries clearly indicate two different cation sites, of which one much prefers ammonium, to the extent that it only half-fills when forced to accept potassium, while the other slightly prefers potassium (see under Experimental). The voids are linked by channels with a height (smallest dimension) equal to the V–F–V distance less twice the pyramidal distortion of the vanadium octahedron and the oxygen radius—about 1Å, which may be insufficient to permit postformation intercalation which is not observed. The voids themselves are somewhat larger whatever their detailed geometry.

It is confusing to find that analytical unipositive cation to fluoride stoichiometry approaches 2:1 and to have to conclude that this deficiency must be made good by hydroxide in materials synthesized under acid conditions. A change in oxidation state of the vanadium is considered highly improbable, not least in view of the clear blue color of these materials, and their tendency to signal even superficial changes by going green. They also hydrolyze to V(IV) in aqueous mineral acid. If correctly identified, these hydroxide ions might be strongly hydrogen-bonded

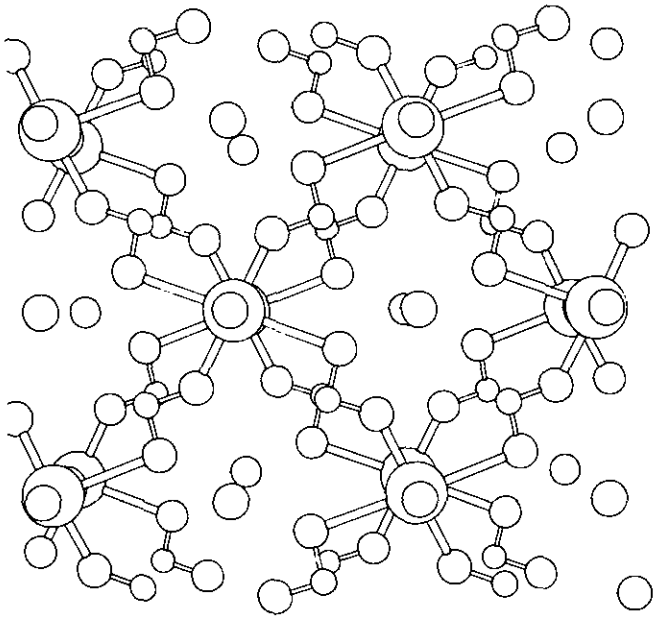

FIG. 5. Proposed voids present in the skeleton of Fig. 4, in the staggered twist version. The voids are bounded above and below by terminal oxygens (shown without their attached vanadium atoms for clarity). The alternative eclipsed twist geometry is not ruled out by the data.

to fluorine, making their infrared diagnostic more difficult. Alternatively one of the ammonium cations might have become NH_3 but this is not supported by the IR, is even less plausible in acid synthesis, and is not applicable to the per-potassium compound.

It has been found helpful to denote layer/double-layer sequences in coded form. The [A] layer, with its associated ligands in the aquo form, becomes [LA] with (vertical) mirror image [ZO], representing geometrical reflection by reflection about the center of the alphabet. The corresponding horizontally translated layers are then [MB] and its reflection [YN]. The simple aquo form sequence is thus [-LAYN-LAYN-LAYN-...] (with dashes representing interlayer hydrogen bonds). The formic acid adduct might be represented by [-LAYN-L′A′Y′N′-LAYN-L′A′Y′N′-LAYN-...], with primes denoting a fundamentally equivalent double layer slightly distorted in geometry and positioning by ligand asymmetry. The fluorides are then [FAYUBZFAYUBZF...], where [U] is the translated fluorine or [F] layer, or [FAYUB″Z″-FAYUB″Z″F...] with double primes representing the staggered twist alternative.

CONCLUSIONS

Some new polymeric oxo-vanadium (IV) materials have been synthesized, in which the planar bidentate formate anion takes the place of the tetrahedral oxo-anion more usually found in comparable high oxidation state transition element compounds. The resulting highly polar sheets interlock into a unique stable double-layer structural unit, already known from the monohydrate. It has been shown by trial simulations that the compounds characterized here are all based on this same double layer, in two different translational relationships. There is evidence for strong cation selectivity during the formation of the variant with interlayer fluorine bridges.

ACKNOWLEDGMENTS

I thank Mike Webster of the Department of Chemistry, University of Southampton for helpful discussions, Ian Thom-Postlethwaite for manual measurement of XRPD intensities ($VO(HCO_2)_2 \cdot HCO_2H$) and A. W. Kirkby for preliminary work. Mark Weller (Department of Chemistry) and Trevor Clayton (Department of Geology) provided XRPD facilities.

REFERENCES

1. (a) A. Leclaire, A. Grandin, J. Chardin, M. M. Borel, and B. Raveau, *Eur. J. Solid State Inorg. Chem.* **30,** 393 (1993); (b) S.-L. Wang and C.-Y. Cheng, *J. Solid State Chem.* **109,** 277 (1994); (c) A. Leclaire, M. M. Borel, A. Grandin, and B. Raveau, *J. Solid State Chem.* **110,** 256 (1994); (d) S.-J. Hwu, R. I. Carroll, and D. L. Serra, *J. Solid State Chem.* **110,** 290 (1994); (e) J. T. Vaughey, W. T. A. Harrison, and A. J. Jacobson, *J. Solid State Chem.* **110,** 305, (1994); (f) M. A. Talbi and R. Brochu, *J. Solid State Chem.* **110,** 350, (1994).
2. A. T. Casey and J. R. Thackray, *Aust. J. Chem.* **22,** 2549, (1969).
3. D. Mootz and R. Seidel, Acta Crystallogr. Sect. C **43,** 1218, (1987).
4. R. Greenhalgh and J. P. Riley, *Anal. Chim. Acta* **25,** 178, (1961).
5. T. R. Gilson, I. M. Thom-Postlethwaite, and M. Webster, *J. Chem. Soc. Dalton Trans.* 895 (1986).
6. T. R. Gilson, unpublished work.
7. M. A. G. Aranda and J. P. Attfield, *Angew. Chem.* **105,** 1511 (1993); (Int. ed.) **32,** 1435 (1993).
8. K. Yvon, W. Jeitschko, and E. Parthé, *J. Appl. Crystallogr.* **10,** 405 (1977).